LES OF MHD TURBULENT TAYLOR-COUETTE FLOW IN AXIAL MAGNETIC FIELD

Hiromichi Kobayashi
Department of Physics, Hiyoshi Campus,
Keio University
4-1-1 Hiyoshi, Kohoku-ku, Yokohama, 223-8521, Japan
hkobayas@keio.jp

Ryo Sasaki
Graduate School of Science and Technology,
University of Tsukuba
1-1-1 Tennodai, Tsukuba, 305-8573, Japan
s2020848@s.tsukuba.ac.jp

Takayasu Fujino
Faculty of Engineering, Information and Systems,
University of Tsukuba
1-1-1 Tennodai, Tsukuba, 305-8573, Japan
tfujino@kz.tsukuba.ac.jp

Hidemasa Takana
Institute of Fluid Science,
Tohoku University
2-1-1 Katahira, Aoba-ku, Sendai, 980-8577, Japan
takana@tohoku.ac.jp

ABSTRACT

Large eddy simulation (LES) of magnetohydrodynamic (MHD) turbulent Taylor-Couette (TC) flows is conducted to reveal the effect of the Hartmann number proportional to the axial magnetic field strength on the flow and electric current fields. The upper-lower walls are insulated and the inner-outer sidewalls are set to insulating walls (open condition) or perfectly conducting walls (short condition). As increasing the Hartmann number, turbulent fluctuations are suppressed, and the turbulent flow distributions approach the MHD laminar flow distributions. The orientations of turbulent vortices change from the azimuthal flow direction to the axial magnetic field direction even in the TC flow. The triplet high-speed streaky structures are uncovered near the inner wall.

INTRODUCTION

Taylor-Couette (TC) flow is one of important and fundamental flows (Coles, 1965; Grossmann *et al.*, 2016) and has been actively studied in various research fields. Direct numerical simulation (DNS) of non-conducting turbulent TC flows has been conducted, and the fine turbulent vortex structures and the turbulence statistics of TC flow are clarified (e.g., see Dong, 2007). The DNS of conducting turbulent TC flows, e.g., liquid metal flows, is performed with conducting sidewalls under the periodic conditions in the azimuthal and axial directions, and the suppression of the fine turbulent vortices is revealed in the axial magnetic field (Leng *et al.*, 2018). When imposing strong magnetic field, it is known that the turbulent vortex is elongated in the direction of the applied magnetic field. The aligned vortex structure is the so-called quasi-two-dimensional (Q2D) structure and appears in magnetohydrodynamic (MHD) flows (e.g., see Chen *et al.*, 2021).

From the viewpoint of the torque control of wind turbine via the Lorentz force and the recovery of excessive wind power as electrical output, Takana & Tanida (2017) has proposed a co-axial MHD energy conversion device and demonstrated the performance in experiments. We conducted the one-dimensional theoretical analysis of the flow field (Sasaki *et al.*, 2021a) and power generation characteristics (Sasaki *et al.*, 2021b). We have already examined two-dimensional MHD laminar TC flows for aspect ratio 10 and exhibited that the number of Taylor vortex gradually diminishes from ten to two as increasing the magnetic field strength (Sasaki *et al.*, 2021c).

In the present study, large eddy simulation (LES) of MHD turbulent TC flows is carried out to clarify the effect of the magnetic field strength on the flow and electric current fields in the MHD energy conversion device.

GOVERNING EQUATIONS AND NUMERICAL CONDITIONS

In this study, LES is conducted to investigate unsteady MHD turbulence structures and laminarization phenomena by the Lorentz force. The low magnetic Reynolds number is assumed. Consequently, induced magnetic fields and the fluctuation of magnetic field are discarded although we can compute the induced magnetic fields as carried out in the previous study (Kobayashi *et al.*, 2012). Governing equations under the low magnetic Reynolds number consit of filtered incompressible Navier-Stokes equations with the Lorentz force, a filtered continuity equation, filtered Maxwell equations and the generalized Ohm's law as described below.

(i) Continuity equation:

$$\nabla \cdot \overline{u} = 0, \tag{1}$$

(ii) Navier-Stokes equations:

$$\frac{\partial \overline{u}}{\partial t} + (\overline{u} \cdot \nabla)\overline{u} = -\frac{1}{\rho}\nabla \overline{p} + \nu \nabla^2 \overline{u} - \nabla \cdot \tau + \frac{1}{\rho}(\overline{j} \times B), \tag{2}$$

(iii) Maxwell equations:

$$\nabla \times \overline{E} = 0, \tag{3}$$

$$\nabla \cdot \overline{j} = 0, \tag{4}$$

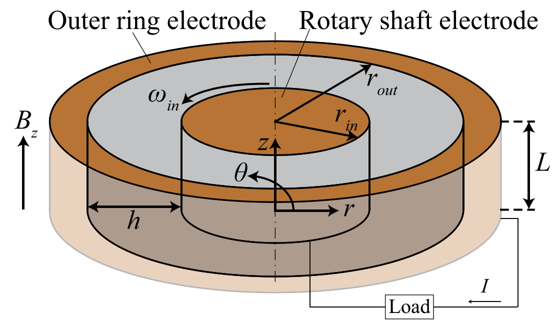

Figure 1. Computational domain where the inner cylindrical electrode is rotating and the outer one is at rest.

(iv) Ohm's law:

$$\overline{j} = \sigma\left(\overline{E} + \overline{u} \times B\right), \tag{5}$$

where $(\bar{\cdot})$ denotes the filtered variable, the velocity $\overline{u} = \overline{u}_i$, the pressure $\overline{p}$, the subgrid-scale (SGS) stress tensor $\tau = \tau_{ij}$, the electric current density $\overline{j}$, the electric field $\overline{E}$ are used. The magnetic flux density B is set to only the external magnetic flux density $(0, 0, B_z)$. The electric potential $\overline{\phi}$ is obtained from the following Poisson equation:

(v) Poisson equation for the electric potential:

$$\nabla^2 \overline{\phi} = \nabla \cdot \left(\overline{u} \times \overline{B}\right), \tag{6}$$

that is derived from eq.(3) - (5).

The equations are discretized in the $r-\theta-z$ cylindrical coordinate. The magnetic field is imposed in the z (axial) direction. We use the second order Adams-Bashforth method for the time marching scheme and the second order central finite difference method for the spatial discretization. The SMAC scheme is used for the coupling between velocity and pressure. We adopt the coherent structure model (Kobayashi, 2005), which is useful subgrid-scale model in the MHD flows (Kobayashi, 2008; Kobayashi *et al.*, 2012).

Figure 1 shows the computational domain. The ratio of the inner radius to the outer radius, namely radius ratio, is set to 0.5. The aspect ratios of 1 and 10 are adopted for the cross section in the $r-z$ plane. We use the insulating walls for the upper and lower walls. We examine two types of the sidewall condition, (1) open condition: insulating sidewalls and (2) short condition: perfectly conducting sidewalls. The no-slip boundary condition is utilized on the walls and no-penetration and penetration wall conditions of electric current are used for open and short conditions, respectively. The computational domain in the azimuthal direction is $\pi/2$ and the periodic boundary condition is adopted. The grid points are set to $(N_r, N_\theta, N_z) = (32, 64, 128)$ because LES of aspect ratio of 10 with those grid points shows good agreement with the mean velocity and turbulent intensity profiles of the DNS (Dong, 2007) (not shown here). Reynolds number is set to 8000. The Hartmann number Ha, the ratio of the Lorentz force to the viscous force, is proportional to the magnetic field strength and is varied from 0 to 100. The Lorentz force acts against the flow and suppresses the turbulence.

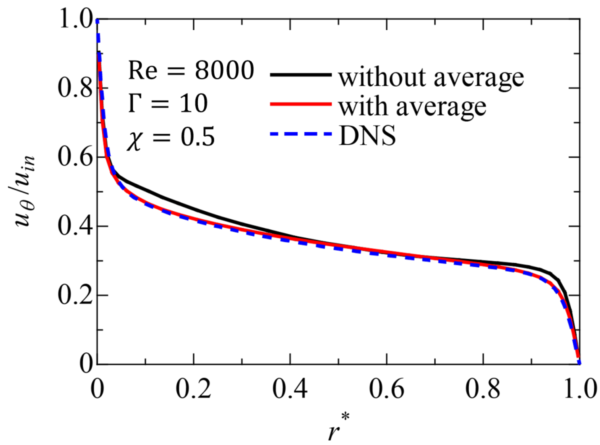

(a) Mean velocity

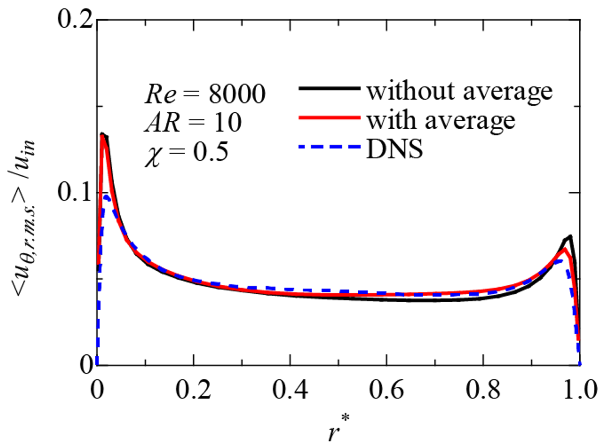

(b) Root mean square velocity

Figure 2. Mean (upper) and root mean square (lower) profiles of azimuthal velocity for the open condition at aspect ratio of 10. The mean velocity with avarage indicates the average in the z direction. The mean velocity without average exhibits the mean velocity at $z = L/2$.

NUMERICAL RESULTS
Results of Aspect Ratio of 10

First, we show the validation results for TC flow of aspect ratio of 10. Figure 2 shows the Mean (upper) and root mean square (lower) profiles of azimuthal velocity for the open condition at aspect ratio of 10. In the present simulation, upper and lower walls exist. Therefore, we showed two mean velocities: with average in the z direction and at $z = L/2$ without average. The mean and root mean square velocity profiles with average are good agreement with the DNS results (Dong, 2007).

Let us see the Taylor vortex cells. In Fig. 3, the mean distributions of stream line and radial velocity for Ha = 0, 50, 70 and 100 of the open condition in the $r-z$ plane at aspect ratio of 10 are displayed. As increasing the Hartmann number, we found that the number of the Taylor vortex or the eddy current is gradually reduced from ten to two. Note that two Taylor vortex cells remains due to the existence of the upper and lower walls even for large Hartmann number.

Figure 4 exhibits the mean distributions of the Joule dissipation and the electric current streamline for $Ha = 70$ and 100 of open and short conditions in the $r-z$ plane at aspect ratio of 10. The cells of electric current streamline are comparable to the Taylor vortex cells for various Hartmann numbers. The Joule dissipation becomes high at the location of the high ra-

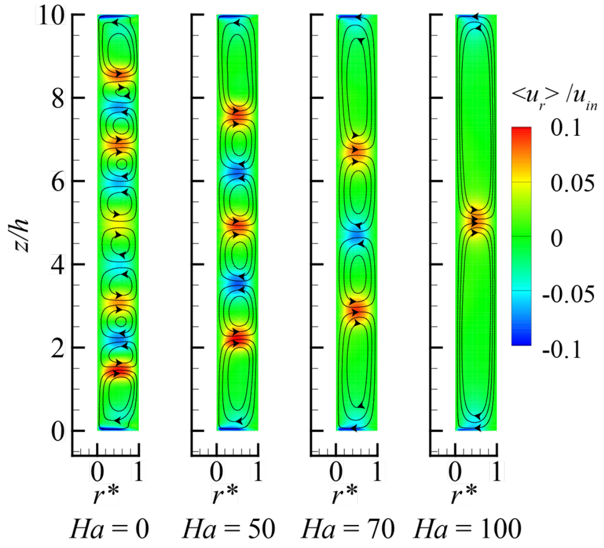

Figure 3. Mean distributions of stream line and radial velocity for $Ha = 0$, 50, 70 and 100 of the open condition in the $r - z$ plane at aspect ratio of 10.

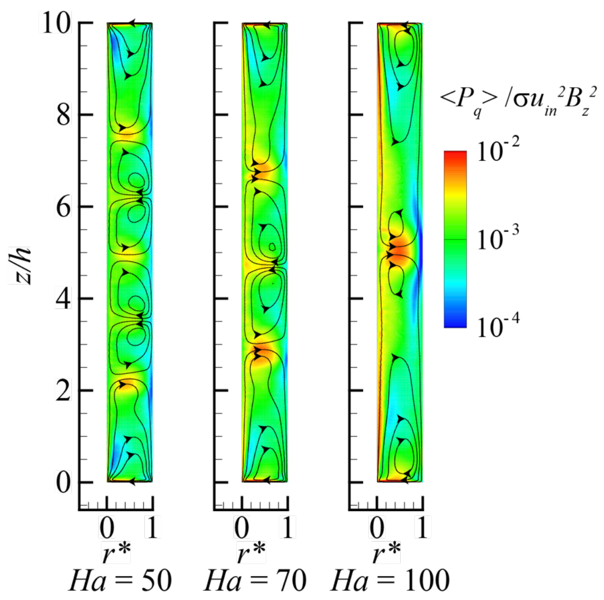

Figure 4. Mean distributions of the Joule dissipation and the electric current streamline for $Ha = 70$ and 100 of open and short conditions in the $r - z$ plane at aspect ratio of 10.

dial velocity as shown in Fig. 3. This is due to the centrifugal force. Owing to the open condition, the electric current flows very close to the wall.

Results of Aspect Ratio of 1

Let us move on to the results of aspect ratio of 1. The mean and root mean square profiles of azimuthal velocity for open and short conditions are shown in Fig. 5. At $Ha = 0$, mean velocity gradient is sharp and the velocity fluctuation is strong near the inner and outer walls. This is the typical turbulent TC statistics (Dong, 2007). When increasing the Hartmann number, the velocity fluctuation is suppressed and then the mean velocity gradient becomes gentle. For the high Hartmann number of the short condition, the mean reverse flow appears on the outer-wall side whereas for that of the open condition the mean reverse flow never emerges on there.

Figure 6 displays the mean distributions of azimuthal velocity and streamline for $Ha = 70$ and 100 of open and short conditions in the $r - z$ plane. Since the upper and lower walls exist, two Taylor vortices appear for the aspect ratio of 1. As increasing the Hartmann number, the Taylor vortices are compressed toward the inner wall owing to the strong Lorentz force.

Figure 7 shows the mean distributions of the Joule dissipation and the electric current streamline for $Ha = 70$ and 100 of open and short conditions in the $r - z$ plane. Under the open condition, eddy currents are induced along the Taylor vortices because all walls are insulated, and electric current cannot penetrate the insulating walls. The electric current concentrates not only near the inner and upper-lower walls but also on the central plane $z/h = 0.5$, so that the high Joule dissipation (in other words Joule heating) occurs there. However, under the short condition, the electric current flows near the upper-lower walls from the inner wall to the outer wall, avoiding the central region where reverse azimuthal velocity appears as shown in Fig. 5(c) and Fig. 6(c)-(d). Moreover, the electric current flows from the inner wall to itself. The current is the so-called short-circuit current. The eddy current and short-circuit current cannot be extracted as electrical output.

Figure 8 exhibits vortex structures extracted by the isosurfaces of the second invariant $Q = 0.25$ of velocity gradient tensor for $Ha = 0$, 50, 70 and 100 of the open condition. At $Ha = 0$, the orientations of the vortices show in the azimuthal direction. At $Ha = 50$, the vortices are suppressed by the Lorentz force. For $Ha = 70$ and 100, the orientations of the vortices change to the axial direction. The vortices are the so-called quasi-two-dimensional (Q2D) vortices that align to the direction of the imposed magnetic field (e.g., see Chen *et al.*, 2021). It is found that the Q2D vortices emerge even in the TC flow.

The contours of instantaneous azimuthal velocity in the vicinity of inner wall for $Ha = 0$, 50, 70 and 100 of the open condition are visualized in Fig. 9. As increasing the Hartmann number, the low-speed streaky structures are curbed. For $Ha = 0$ and 30, the high and low-speed streaky structures are advected with the flow velocity. For $Ha = 70$ and 100, the high-speed streaky structures have triplet structures and move slowly although the flow velocities near the inner wall are higher than those for $Ha = 0$ and 50 as shown in Fig. 5(a). The slow velocity may correspond to a group velocity. It will be investigated in more dial.

CONCLUSIONS

We conducted the LES of MHD turbulent TC flows and investigated the effect of the Hartmann number on the velocity and electric current distributions. When increasing the Hartmann number, turbulent fluctuations are suppressed, and the velocity and electric current distributions approach the MHD laminar flow distributions. For high Hartmann numbers, two Taylor vortices appear, and the eddy currents for the open condition or the short-circuit currents for the short condition are induced along the TC vortices. The fine turbulent vortices orientating in the azimuthal direction for no magnetic field align in the axial magnetic field direction, so that we found that the Q2D structures appear even in TC flow. The triplet high-speed streaky structures are discovered for high Hartmann numbers and are transported slowly in the azimuthal (flow) direction.

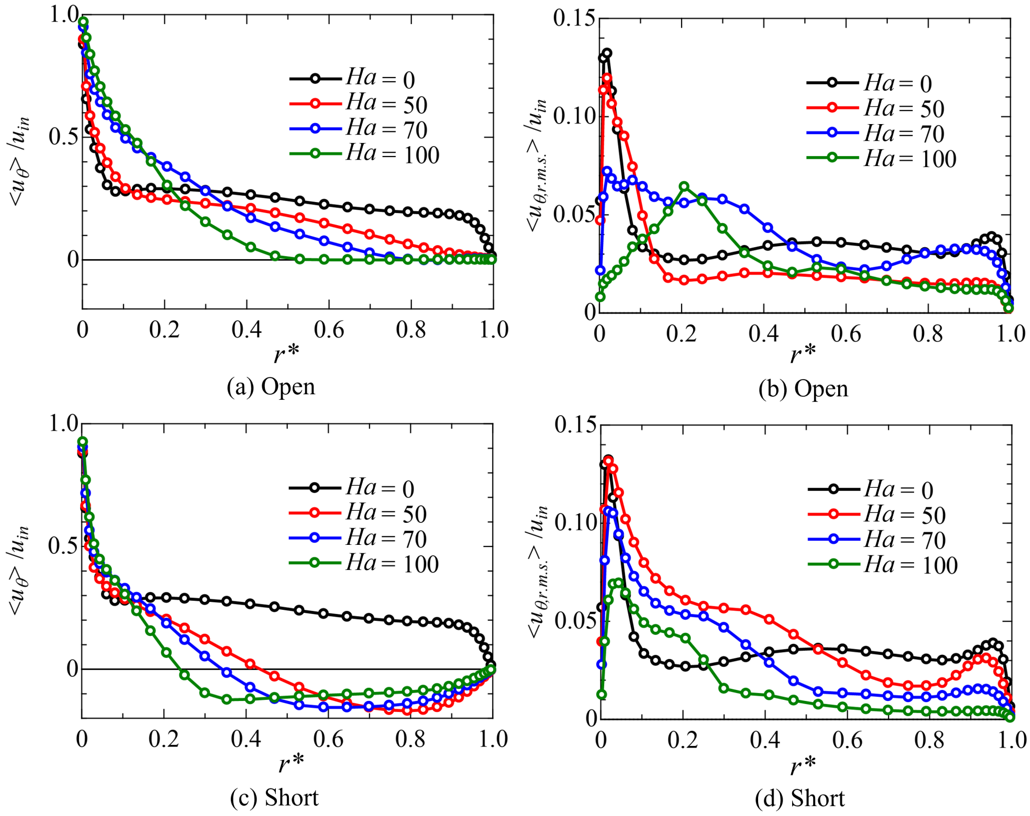

Figure 5. Mean (left) and root mean square (right) profiles of azimuthal velocity for open (upper) and short (lower) conditions.

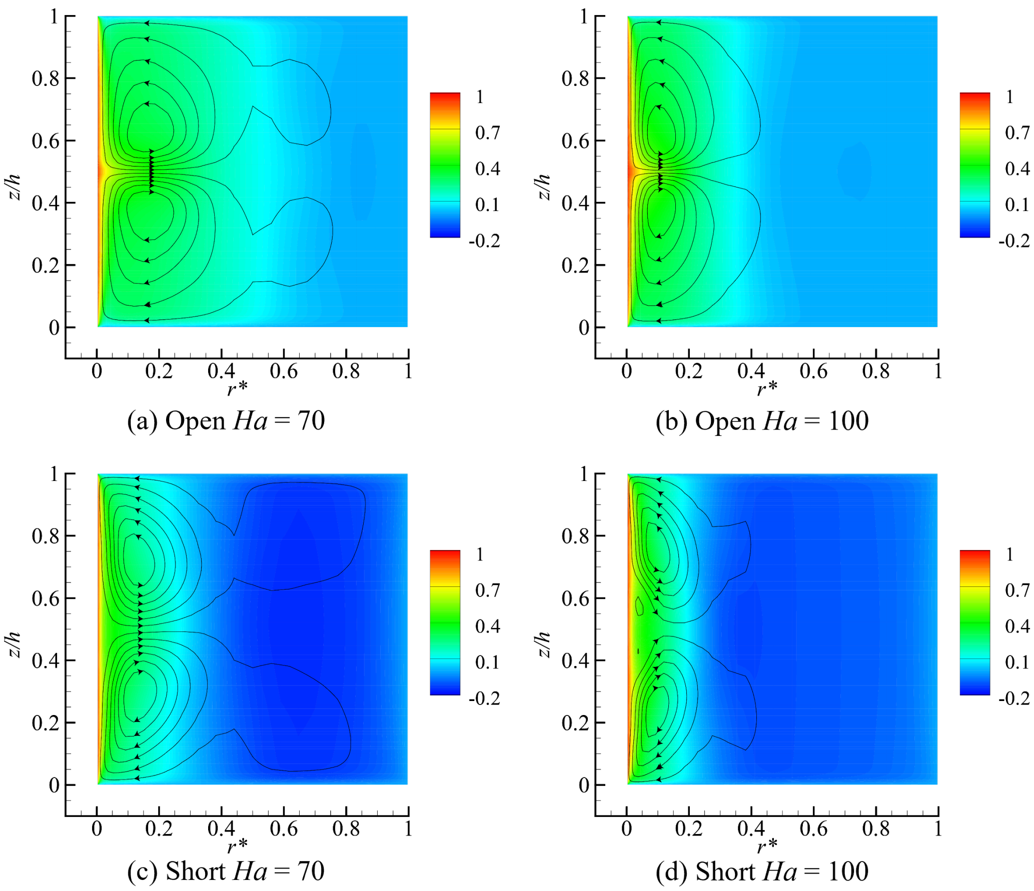

Figure 6. Mean distributions of azimuthal velocity and streamline for $Ha = 70$ and 100 of open and short conditions in the $r - z$ plane.

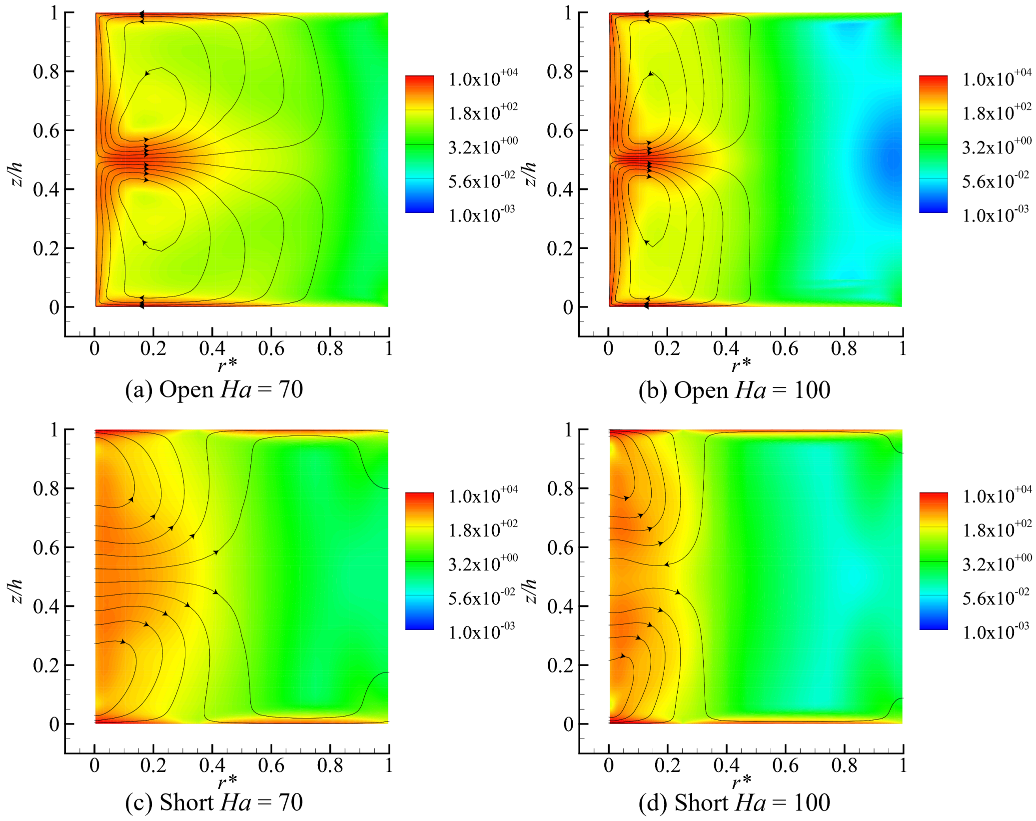

Figure 7. Mean distributions of Joule dissipation and electric current streamline for $Ha = 70$ and 100 of open and short conditions in the $r-z$ plane.

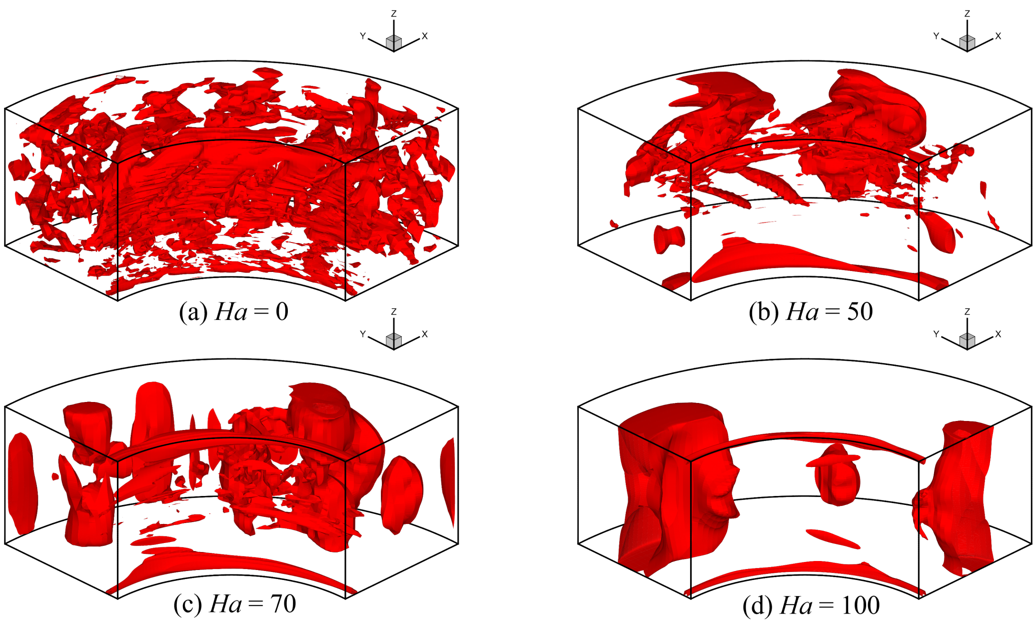

Figure 8. Iso-surfaces of the second invariant $Q = 0.25$ of velocity gradient tensor for $Ha = 0$, 50, 70 and 100 of the open condition.

REFERENCES

Chen, L., Potherat, A., Ni, M-J. & Moreau, R. 2021 Direct numerical simulation of quasi-two-dimensional MHD turbulent shear flows. *J. Fluid Mech.* **915**, A130.

Coles, D. 1965 Transition in circular Couette flow. *J. Fluid Mech.* **21**, 385–425.

Dong, S. 2007 Direct numerical simulation of turbulent Taylor-Couette flow. *J. Fluid Mech.* **587**, 373–393.

Grossmann, S., Lohse, D. & Sun, C. 2016 High-Reynolds number Taylor-Couette turbulence. *Annu. Rev. Fluid Mech.* **48**, 53–80.

Kobayashi, H. 2005 The subgrid-scale models based on co-

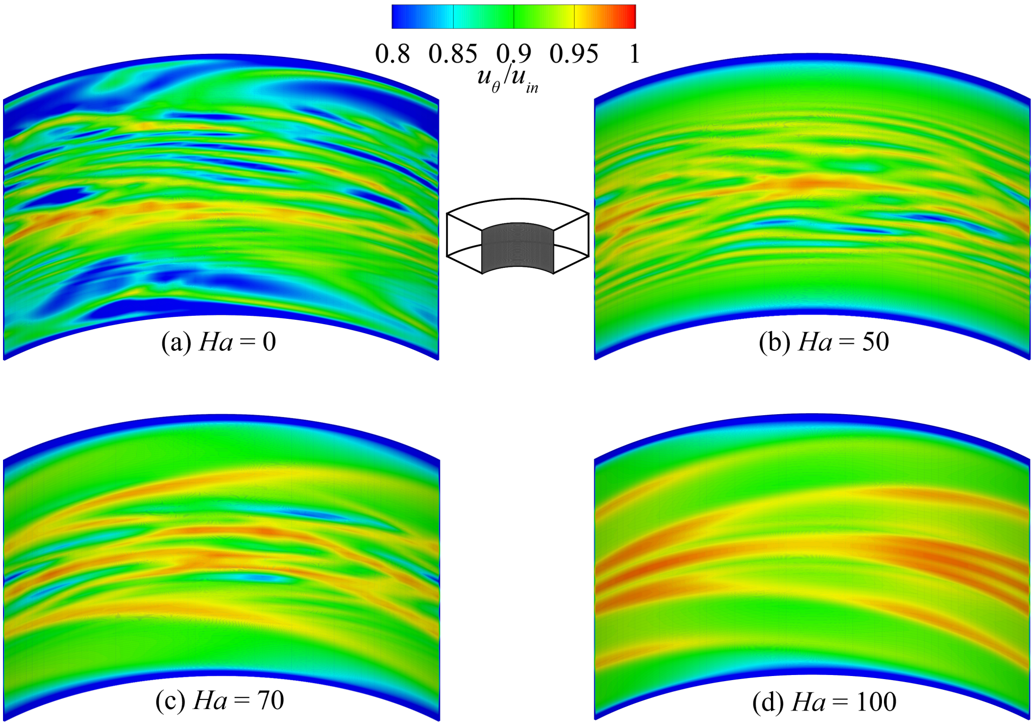

Figure 9. Contours of instantaneous azimuthal velocity in the vicinity of inner wall for $Ha = 0$, 50, 70 and 100 of the open condition.

herent structures for rotating homogeneous turbulence and turbulent channel flow. *Phys. Fluids* **17**, 045104.

KOBAYASHI, H. 2008 Large eddy simulation of magnetohydrodynamic turbulent duct flows. *Phys. Fluids* **20**, 015102.

KOBAYASHI, H., SHIONOYA, H. & OKUNO, Y. 2012 Turbulent duct flows in a liquid metal magnetohydrodynamic power generator. *J. Fluid Mech.* **713**, 243–270.

LENG, X., KOLESNIKOV, Y.B., KRASNOV,D., & LI, B. 2018 Numerical simulation of turbulent Taylor-Couette flow between conducting cylinders in an axial magnetic field at low magnetic Reynolds number. *Phys. Fluids* **30**, 015107.

SASAKI, R., FUJINO, T., TAKANA, H. & KOBAYASHI, H. 2021 Theoretical analysis of annular laminar flows with MHD interaction driven by rotating co-axial cylinder. *Electron Comm. Jpn.* **104**, No. 2, pp. 1-9.

SASAKI, R., FUJINO, T., TAKANA, H. & KOBAYASHI, H. 2021 Theoretical analysis on power generation characteristics for co-axial MHD energy conversion device. *IEEJ Trans. Power Energy* **14**, No. 10, pp. 642-648 (in Japanese).

SASAKI, R., FUJINO, T., TAKANA, H. & KOBAYASHI, H. 2021 Quasi-two-dimensional numerical analysis of influence of taylor vortex and eddy current on generation characteristics of co-axial MHD energy conversion device under laminar flow. *IEEJ Trans. Power Energy* (in Japanese) (to be published).

TAKANA, H. & TANIDA, A. 2017 Development and fundamental characteristics of co-axial MHD energy conversion device. *Mech. Eng. Journal* **4**, No. 1, 16-00500.